JOURNAL OF GEOPHYSICAL RESEARCH, VOL. 115, D02114, doi:10.1029/2009JD012097, 2010

Performance of high-resolution satellite precipitation products over China

Yan Shen,[1] Anyuan Xiong,[1] Ying Wang,[1] and Pingping Xie[2]

Received 19 March 2009; revised 31 August 2009; accepted 15 September 2009; published 30 January 2010.

[1] A gauge-based analysis of hourly precipitation is constructed on a 0.25° latitude/longitude grid over China for a 3 year period from 2005 to 2007 by interpolating gauge reports from ~2000 stations collected and quality controlled by the National Meteorological Information Center of the China Meteorological Administration. Gauge-based precipitation analysis is applied to examine the performance of six high-resolution satellite precipitation estimates, including Joyce et al.'s (2004) Climate Prediction Center Morphing Technique (CMORPH) and the arithmetic mean of the microwave estimates used in CMORPH; Huffman et al.'s (2007) Tropical Rainfall Measuring Mission (TRMM) precipitation product 3B42 and its real-time version 3B42RT; Turk et al.'s (2004) Naval Research Laboratory blended product; and Hsu et al.'s (1997) Precipitation Estimation From Remotely Sensed Information Using Artificial Neural Network (PERSIANN). Our results showed the following: (1) all six satellite products are capable of capturing the overall spatial distribution and temporal variations of precipitation reasonably well; (2) performance of the satellite products varies for different regions and different precipitation regimes, with better comparison statistics observed over wet regions and for warm seasons; (3) products based solely on satellite observations present regionally and seasonally varying biases, while the gauge-adjustment procedures applied in TRMM 3B42 remove the large-scale bias almost completely; (4) CMORPH exhibits the best performance in depicting the spatial pattern and temporal variations of precipitation; and (5) both the relative magnitude and the phase of the warm season precipitation over China are estimated quite well, but the early morning peak associated with the Mei-Yu rainfall over central eastern China is substantially under-estimated by all satellite products.

Citation: Shen, Y., A. Xiong, Y. Wang, and P. Xie (2010), Performance of high-resolution satellite precipitation products over China, *J. Geophys. Res.*, *115*, D02114, doi:10.1029/2009JD012097.

1. Introduction

[2] Despite its crucial importance in many meteorological, hydrological, and water resources management applications, accurate documentation of regional and global precipitation remains a challenging task. In particular, precipitation variations on subdaily time scales, which represent a substantial portion of precipitation variability and play an important role in hydrological cycle and land-atmosphere interactions [*Dai et al.*, 1999], are not well observed over most of the globe. Gauge observations provide relatively accurate measurements of precipitation at the station locations. Gauge observation records for precipitation of subdaily accumulations, however, are only available over several regions over land (e.g., the contiguous Unites States; see *Higgins et al.* [1996]). In addition, quality of gauge-based analysis of precipitation depends on the configuration and density of the gauge station networks which, over some regions, are insufficient for monitoring of subdaily precipitation variations associated with mesoscale systems [*Morrissey et al.*, 1995].

[3] Estimates of precipitation have been derived from satellite observations of infrared (IR; see *Arkin and Meisner* [1987], *Susskind et al.* [1997], and *Xie and Arkin* [1998]), passive microwave (PMW; see *Wilheit et al.* [1991], *Spencer* [1993], and *Ferraro* [1997]), and spaceborne precipitation radar (PR; see *Kummerow et al.* [2000]). While precipitation products based on observations from individual instruments have been widely utilized in a variety of operational and research applications, integrating information from multiple satellite sensors as well as gauge observations further improves the quality and resolution of precipitation analysis. Substantial progress has been made in the past decade to generate precipitation estimates of high spatial and temporal resolution through combined use of infrared (IR) and passive microwave (PMW) observations from multiple satellites. *Hsu et al.* [1997] constructed a sophisticated system to convert the IR brightness temperatures observed

[1]National Meteorological Information Center, China Meteorological Administration, Beijing, China.
[2]NOAA Climate Prediction Center, Camp Springs, Maryland, USA.

0148-0227/10/2009JD012097$09.00

by geostationary satellites into instantaneous rain rates through an artificial neural network trained carefully using concurrent IR- and PMW-based precipitation estimates. *Turk et al.* [2004] and *Huffman et al.* [2007] developed their algorithms to derive IR-based precipitation estimates through matching the probability density function (PDF) of the geostationary IR data with that of the precipitation intensity from the colocated PMW estimates and then combine these IR-based estimates with PMW data to form precipitation maps of high spatial/temporal resolution. The technique of *Joyce et al.* [2004], meanwhile, defines the precipitation analysis in 30 min intervals and on an 8 km by 8 km grid over the globe through propagating the precipitating cloud clusters observed by the instantaneous PMW estimates along the advection vectors computed from consecutive geostationary IR images. A similar Lagrangian approach is adopted by *Ushio et al.* [2009], who developed a Kalman filtering–based method to construct maps of hourly precipitation on a 0.25° latitude/longitude grid over the globe.

[4] These high-resolution satellite precipitation products have been used in a wide range of applications, including weather/climate monitoring, climate analysis, numerical model verifications, and hydrological studies [e.g., *Sorooshian et al.*, 2002; *Hossain and Anagnostou*, 2004; *Gottschalck et al.*, 2005; *Janowiak et al.*, 2005; *Yang and Smith*, 2006; *Dai*, 2006; *Dai et al.*, 2007; *Yu et al.*, 2007a, 2007b]. In particular, the very high spatial and temporal resolution of the satellite products enables the examination of diurnal variations of precipitation and the associated mesoscale cloud/precipitation systems. *Yang and Smith* [2006] investigated the characteristics and mechanisms of diurnal cycle of precipitation over various parts of the globe using precipitation retrievals from three TRMM level 2 products (the TMI-only 3B12, PR-only 3B25, and TMI/PR combined 3B31). *Dai et al.* [2007] performed a comprehensive examination of the frequency, intensity, and diurnal cycle of precipitation over the globe using surface observations and satellite estimates of PERSIANN, CMORPH, and TRMM 3B42, and confirmed early findings that oceanic precipitation exhibits an early morning maximum while over most land areas warm season precipitation peaks in late afternoon. *Zhou et al.* [2008] compared the diurnal cycle of warm season precipitation over the contiguous China estimated by the PERSIANN and TRMM 3B42 products with that observed by gauge observations and found that the satellite products overestimate the frequency but under-estimate the intensity of rainfall over eastern China.

[5] Uncertainties, however, exist in the accuracy of the high-resolution satellite precipitation products in representing the spatial distribution, temporal variations, and frequency of precipitation, and need to be examined for the further improvements of the construction algorithms and appropriate quantitative applications of the products. *Gottschalck et al.* [2005] compared satellite-based estimates, satellite-gauge merged analyses and model-generated precipitation fields with the daily precipitation analysis of *Higgins et al.* [2000] on the basis of stations reports from a very dense network of gauges over the contiguous United States (CONUS) and found that satellite-based products of PERSIANN and TRMM 3B42 exhibit the best performance during summer but tend to overestimate the precipitation. In a comparison against their gauge-based analysis of daily precipitation over China, *Xie et al.* [2007] revealed that high-resolution satellite precipitation products perform better over areas of wet climate and that bias in the satellite products is removed substantially when they are blended with gauge observations. Furthermore, *Ebert et al.* [2007] reported a comprehensive examination of twelve satellite- and model-based precipitation products through comparison with gauge-based analyses of daily precipitation over CONUS, Australia and Europe.

[6] All above mentioned studies addressed the skills of the high-resolution precipitation products in estimating precipitation variations of daily and longer time scales. Performance of these satellite products in reproducing variations of subdaily time scales is largely unknown over the most of the globe owing to the lack of in situ observations over large spatial domains and covering extensive time periods with the required time resolution. Several studies have compared diurnal variations of precipitation derived from satellite products against those from the hourly gauge analysis of *Higgins et al.* [1996] over CONUS [*Dai et al.*, 2007; *Tian et al.*, 2007], and those from the NAME event gauge network over Mexico [*Hong et al.*, 2007]. *Zhou et al.* [2008] investigated the performance of several satellite products using station reports of hourly precipitation over China.

[7] Recently, the National Meteorological Information Center (NMIC) of the China Meteorological Administration (CMA) started to collect, digitalize and perform quality control for hourly precipitation reports from over 2000 automatic weather stations over China on a quasi real-time basis. An objective analysis system has been developed to create gridded analysis of hourly precipitation on a 0.25° latitude/longitude grid over China. Taking advantage of this gauge analysis, we will examine the performance of six satellite-based high-resolution precipitation products in estimating precipitation variations on time scales from 3 hourly to daily. Our study will assess the skills of these satellite products in reproducing the spatial distribution, temporal variations and the frequency of precipitation events with various intensities.

[8] This paper is organized into five parts. Section 2 describes the gauge-based analysis of hourly precipitation over China; section 3 introduces the six high-resolution satellite precipitation products to be examined in this study; section 4 documents the assessment results of the satellite products against the gauge analysis; and a summary will be given in section 5.

2. Gauge-Based Analysis of Hourly Precipitation Over China

[9] Gauge observations play a critical role in the quantitative documentation of precipitation over land. While information on precipitation can also be collected from estimates derived from satellite observations and fields generated by various numerical models, they are indirect in nature and need to be calibrated or examined using the gauge observations [*Ebert and Manton*, 1998; *Adler et al.*, 2001; *McCollum et al.*, 2002]. In the past two decades, gauge-based analyses of monthly climatology, monthly and

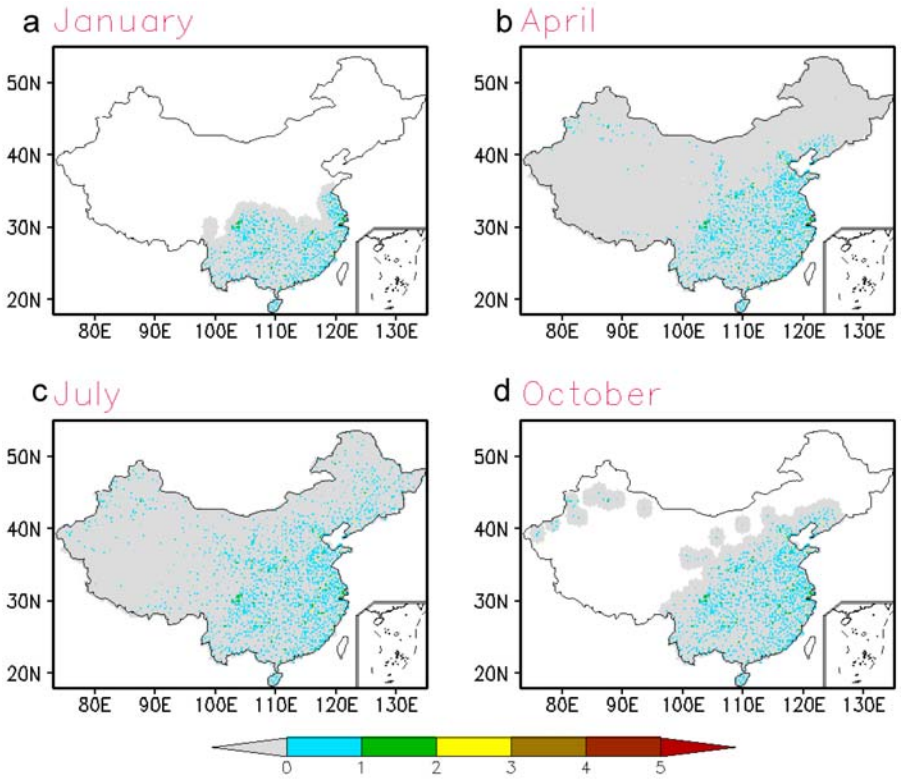

Figure 1. Number of gauges in a 0.25° latitude/longitude grid box for (a) January, (b) April, (c) July, and (d) October. Shaded areas indicate regions over which hourly precipitation measurements from automatic rain gauges are performed.

daily precipitation time series have been constructed over global land and regional domains by interpolating corresponding station reports [*Legates and Willmott*, 1990; *Hulme*, 1991; *Schneider et al.*, 1993; *Xie et al.*, 1996, 2007; *Dai et al.*, 1997; *New et al.*, 1999, 2000; *Higgins et al.*, 2000; *Chen et al.*, 2002].

[10] Gauge-based analyses of precipitation on subdaily time scales are rarely available because precipitation measurements are made at subdaily intervals only at a limited number of stations over a selection of regions and that access to these station reports is often restricted from many countries. One of the more widely used subdaily precipitation data sets is the CONUS hourly gauge-based analysis of *Higgins et al.* [1996] created for a 45 year period from 1963 to the present by interpolating gauge reports at over 3000 stations collected in the TD-3240 data set [*Hammer and Steurer*, 1997] of the NOAA National Climatic Data Center (NCDC). Despite its coarse resolution of 2.5° longitude by 2.0° latitude, the hourly gauge-based analysis has been widely utilized in climate diagnostics, model verifications and satellite products assessments associated with diurnal variations of precipitation [e.g., *Dai et al.*, 1999; *Nesbitt and Zipser*, 2003; *Liang et al.*, 2004].

[11] Recently a project has been launched at CMA/NMIC to create a comprehensive database of gauge-observed hourly precipitation reports from a national network of ~2000 automatic weather stations. Hourly precipitation is measured by siphon or tipping-bucket rain gauges and recoded automatically. Hourly precipitation reports from these automatic stations are transferred to CMA/NMIC where a three level quality control procedure is applied to flag and remove bad reports through (1) the extreme check, (2) internal consistency check, and (3) spatial consistency check. The extreme check is conducted by comparison with the maximum of the daily precipitation time series for the target month. Reports of daily precipitation at many stations are collected at manned meteorological stations and go through manual quality check. An hourly report is rejected if its value exceeds the monthly maximum of daily precipitation. The internal consistency check is designed to identify erroneous reports caused by incorrect units, reading, or coding. The spatial consistency check compares the time series of hourly precipitation at the target station with those from nearby stations. Overall, less than 0.1% of the total hourly precipitation reports are rejected in these quality control procedures. As of July 2008 when this work started, quality controlled hourly precipitation reports are available for a 3 year period from 2005 to 2007. As a first step of this study, we generated a gauge-based analysis of hourly precipitation on a 0.25° latitude/longitude grid over the contiguous China for the 3 year period through interpolation of the quality controlled station reports.

[12] The Chinese hourly gauge network consists of a total of ~2000 stations distributed unevenly over China (Figure 1). About 80% of the stations are located over the eastern half of the country where the climate is wet and the population is concentrated. The gauge network is very sparse over the arid and semiarid regions of western China. While hourly precipitation is measured by automatic rain gauges, most stations over northern China operate only

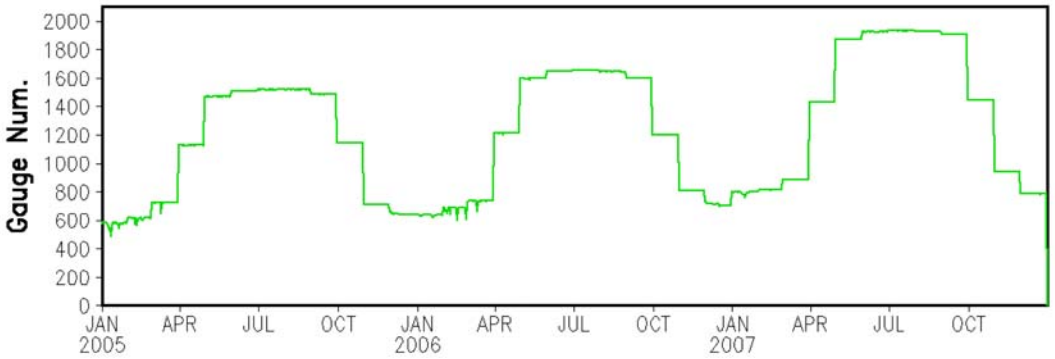

Figure 2. Number of Chinese stations reporting hourly precipitation over a 3 year period from January 2005 to December 2007.

during the warm seasons (Figure 1), yielding a seasonal variation of reporting station numbers (Figure 2). The number of available hourly precipitation reports reaches its maximum/minimum of ~1800/~600, respectively, during summer and winter.

[13] The algorithm used to define the analyzed fields of hourly precipitation over China is an adaptation of the objective technique of *Xie et al.* [2007] developed originally for the construction of daily precipitation analysis over East Asia. First, analyzed fields of daily precipitation climatology are computed by interpolating station climatology defined as the summation of the first six harmonics of the 365 calendar day time series of the mean daily values averaged over a 30 year period from 1971 to 2000. These fields of daily climatology are then adjusted by the Parameter-Elevation Regression on Independent Slopes Model (PRISM) monthly precipitation climatology of *Daly et al.* [1994] to correct the bias caused by orographic effects. Gridded fields of the ratio of hourly precipitation to the daily climatology are created by interpolating the corresponding station values using the optimal interpolation (OI) method of *Gandin* [1965]. Analyses of hourly precipitation are finally calculated by multiplying the daily climatology by the hourly ratio.

[14] Orographic effects in precipitation present substantial diurnal variations [*Yu et al.*, 2004, 2007a, 2007b; *Hong et al.*, 2007]. The precipitation climatology used in the interpolation algorithm to represent the orographic effects therefore needs to reflect the diurnal variations in defining the precipitation analysis of subdaily time scales. This is particularly important over regions of substantial diurnal changes in the orographic effects but covered with poor station networks. Diurnal variations of precipitation in the analysis will be smoothed by interpolation of station reports from remote stations using climatology of daily precipitation as the first guess. A precipitation climatology resolving diurnal variations over China, however, was not available when we constructed the hourly gauge analysis. The daily precipitation climatology defined in the work of *Xie et al.* [2007] is utilized instead to account for the overall effects of orographic enhancements in precipitation in creating the current version of the gauge-based analysis of hourly precipitation over China.

[15] The gauge-based analysis of hourly precipitation is constructed on a 0.25° latitude/longitude grid over China for a 3 year period from 2005 to 2007 by interpolating station reports using the algorithm described above. In addition to the analyzed fields of hourly precipitation, the number of reporting stations available inside each 0.25° latitude/longitude grid box is also included as a proxy index of the analysis quality. Figure 3 illustrates an example of the hourly precipitation analysis for 0000 UT on 1 June 2005 (Figure 3, top), and the distribution of reporting station number in a 0.25° latitude/longitude grid used to define the analysis. Precipitating systems are well captured by the hourly gauge analysis over eastern China where station network is relatively dense, while patterns of precipitation may be distorted over western China where analyzed values are defined by interpolation of reports from distant stations.

[16] Precipitation analyses of longer temporal resolutions (3 hourly, 6 hourly, and daily) are defined by accumulating the hourly analysis over the corresponding periods and used as the "ground truth" to verify the satellite-based precipitation estimates. Although interpolating station reports for a longer accumulation period (e.g., 3 h) generally yields analyses of better quantitative accuracy, our preliminary inspections showed only minor differences in most cases, especially over grid boxes with at least one station report.

3. Satellite High-Resolution Precipitation Products

[17] The satellite products to be examined here include (1) Precipitation Estimation From Remotely Sensed Information Using Artificial Neural Network (PERSIANN; see *Hsu et al.* [1997]); (2) the Naval Research Laboratory (NRL) blended satellite precipitation estimates; [*Turk et al.*, 2004]; (3) Tropical Rainfall Measuring Mission (TRMM) precipitation products 3B42 version 6 and (4) its real-time version 3B42RT [*Huffman et al.*, 2007]; (5) global precipitation fields generated by the NOAA CPC morphing technique (CMORPH; see *Joyce et al.* [2004]); and (6) simple average of the microwave-based estimates used in creating the CMORPH (MWCOMB).

[18] The above mentioned high-resolution precipitation products are all defined through combining information derived from passive microwave (PMW) observations aboard low-orbit platforms and infrared (IR) observations from geostationary satellites. PMW measurements provide infrequent but relatively accurate estimates of instantaneous

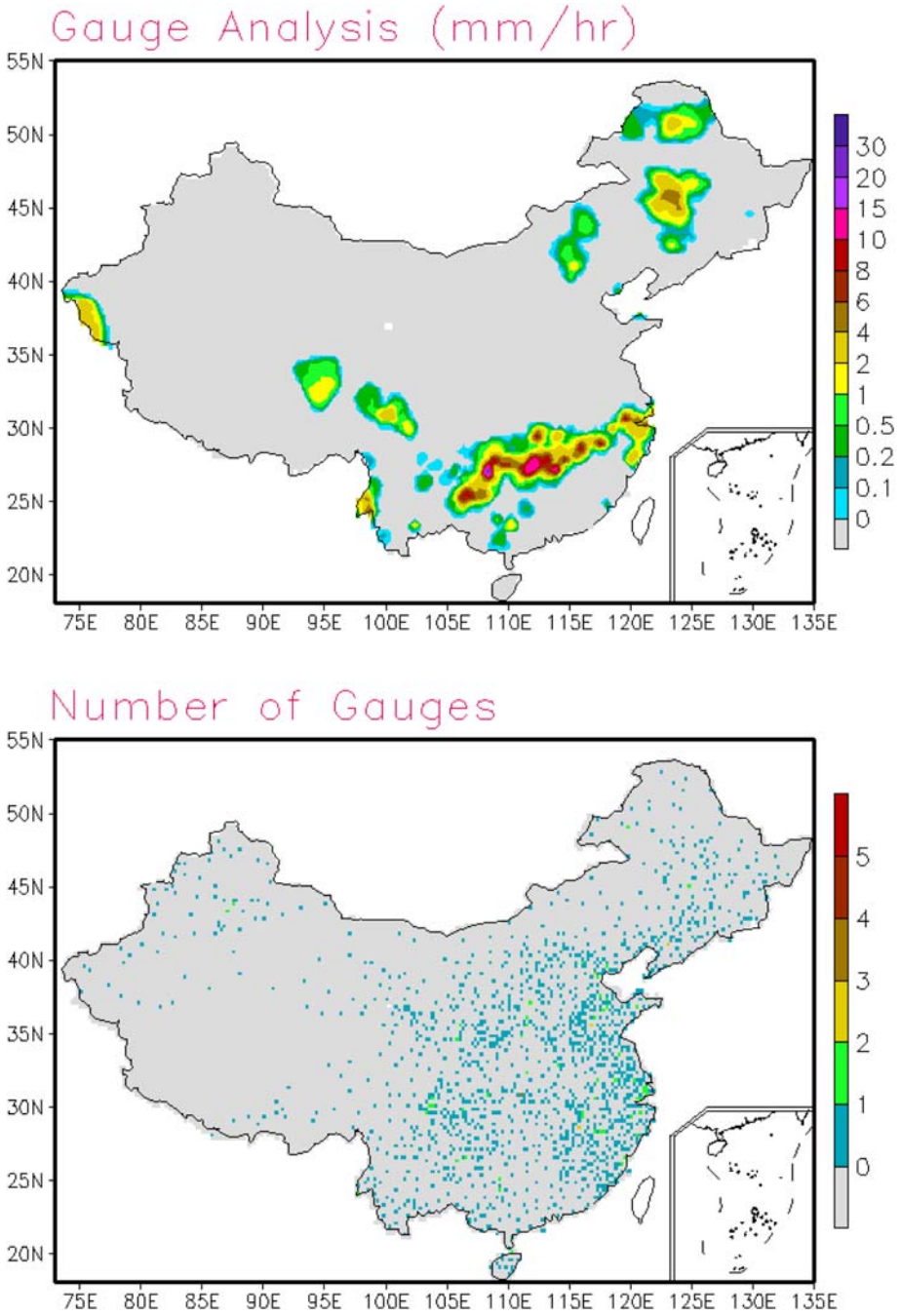

Figure 3. (top) Sample gauge-based analysis of hourly precipitation (mm) for 0000 UT on 1 June 2005 and (bottom) number of gauge reports used to define the analysis.

precipitation rates. The geostationary IR observations, meanwhile, offer frequent sampling of clouds and their movements from which information on precipitation may be derived.

[19] In PERSIANN, NRL and TRMM 3B42RT, a temporally changing local relationship between the precipitation rates and the IR brightness temperature is established using colocated PMW precipitation estimates and geostationary IR data, assuming that the PMW estimates are accurate enough to represent the ground truth of instantaneous precipitation rates. In the PERSIANN, precipitation-IR relationship is created through an artificial neural network [*Hsu et al.*, 1997]. In the NRL and TRMM 3B42RT, this relationship is defined through matching the probability density function (PDF) of the PMW estimates with that of the IR brightness temperatures [*Turk et al.*, 2004; *Huffman et al.*, 2007]. In the NRL and TRMM 3B42RT, this IR-based precipitation fields are then blended with the PMW precipitation estimates to define the final blended products of global precipitation, while in the PERSIANN no further blending of the PMW estimates is performed. The PERSIANN offers hourly precipitation estimates on a 0.25° latitude/longitude grid over the globe (60°S–60°N) from March 2000. The NRL blended products of 3 hourly precipitation are generated

on a 0.25° latitude/longitude grid over the globe (60°S–60°N) for a 6 year period from April 2003, while TRMM 3B42RT products are constructed on a 0.25° latitude/longitude over the globe (50°S–50°N) in 3 hourly intervals covering the entire TRMM observation period starting from January 1998. The TRMM 3B42RT to be examined in this study is version 6.

[20] CMORPH takes a Lagrangian approach to construct high-resolution global precipitation maps from the satellite IR and PMW observation data [*Joyce et al.*, 2004]. First, advection vectors of cloud and precipitation systems are computed using consecutive geostationary IR images in 30 min intervals. These advection vectors are then applied to propagate the precipitating cloud systems observed by the PMW measurements from low-orbit platforms along the advection vectors in both forward and backward directions toward the target time of the precipitation analysis. The final precipitation analysis value at a grid box is defined as the weighted mean of the estimates from the forward and backward propagations with the weights inversely proportional to the time separation between the target analysis time and the PWM observations. As of July 2008, CMORPH precipitation estimates are generated on an 8 km by 8 km resolution over the globe (60°S–60°N) in 30 min temporal resolution from December 2002 to the present.

[21] The MWCOMB is an accompanying product of CMORPH defined as the arithmetic mean of the PMW estimates used as inputs to the CMORPH. Comparisons between the CMORPH and the MWCOMB provide insights into to what extent precipitation estimates may be improved by the morphing processes compared to simply taking arithmetic mean of the inputs. The MWCOMB provides 3 hourly precipitation estimates on a 0.25° latitude/longitude grid over the globe (60°S–60°N) covering the same time period as that for the CMORPH.

[22] All of the five products introduced above (PERSIANN, NRL, TRMM 3B42, CMORPH, and MWCOMB) are based solely on satellite observations. The TRMM 3B42 further combines the information from gauge observations to remove the bias in the satellite estimates. Generated on a postprocessing mode, the TRMM 3B42 is created by adjusting the all-satellite 3 hourly precipitation products similar to the real-time product of 3B42RT using the GPCC gauge-based analysis of monthly precipitation [*Huffman et al.*, 2007]. The time/space resolution and coverage of the TRMM 3B42 is the same as that of the TRMM 3B42RT. The version 6 data set is utilized in this work.

[23] On the basis of the different combinations of information used as inputs, the six high-resolution satellite precipitation products to be examined here can be categorized into three groups; that is, (1) the PMW-only MWCOMB; (2) the satellite observation, only PERSIANN, NRL, TRMM 3B42RT, and CMORPH; and (3) the gauge-adjusted TRMM 3B42. We will consider the impacts of input information in analyzing the evaluation results for the satellite precipitation products.

[24] To assess the performance of the six high-resolution products, precipitation estimates of original resolutions (as described in the early portion of section 3) over China are extracted from the global domain. Three-hourly precipitation data are computed on a 0.25° latitude/longitude grid. The extracted data domain covers an area of 70° longitude by 35° latitude (70–140°E; 15–50°N) and the target time period extends from 2005 to 2007, the 3 year duration for which the gauge-based hourly precipitation analysis is available.

[25] Special cautions have been taken to integrate the gauge-based analysis of hourly precipitation described in section 2 into 3 hourly accumulations that match the time period definition of the satellite estimates. Three-hourly precipitation estimates derived from the PERSIANN, NRL, CMORPH and MWCOMB are defined as the mean precipitation rates for 3 hourly periods starting/ending at 0000, 0300, 0600, 0900, 1200, 1500, 1800, and 2100 UT. Matching gauge analysis is computed simply by averaging the 3 hourly values falling into the time period. The precipitation estimates generated by the TRMM 3B42 and 3B42RT, however, are the mean rain rates over 3 hourly periods centered at the time points. A separate set of 3 hourly gauge analysis is created by computing the 3 hourly value as a weighted mean of the 4 hourly values falling completely or partially into the target time period with the weight proportional to the fraction of the hourly box inside the 3 hourly period. For example, the gauge analysis for a 3 hourly box centering at 0300 UT is defined by averaging hourly values ending at 0200, 0300, 0400, and 0500 UT, with weights of 0.5, 1.0, 1.0, and 0.5, respectively. Without gauge observations in 30 min or finer temporal resolution, this weighted averaging yields improved representation of the 3 hourly precipitation close to what the TRMM products represent.

4. Assessment Results

[26] The six sets of high-resolution satellite precipitation products are compared against our newly created gauge-based analysis of hourly precipitation over China for a 3 year period from 2005 to 2007. Examining satellite estimates of precipitation through comparisons with gauge observations is complicated by impact matching in space and time. In general, satellite estimates of precipitation are derived from instantaneous observations covering the target area and measured during the target time period. Gauges, meanwhile, measure the amount of precipitation accumulated over the target period at the gauge locations. The differences between the satellite estimated and gauge measured precipitation amounts are caused by (1) satellite sampling error, (2) satellite retrieval (estimation) error, and (3) gauge spatial sampling error [*Serra and McPhaden*, 2003; *Bowman*, 2005]. To accurately assess the satellite estimation error, gauge and satellite sampling error need to be quantified using statistical properties of the target precipitation fields [*Bell and Kundu*, 2003; *Bowman et al.*, 2003].

[27] In this study we are trying to evaluate the performance of high-resolution precipitation products defined by combining estimates from individual satellites. Error in these products is attributable to multiple factors including satellite sampling error, retrieval errors of precipitation estimates from individual satellite platforms, and error in integrating individual estimates into the combined precipitation fields. The purpose of this study, however, is to assess the overall performance of the selected satellite products in representing the amount and variations of precipitation over a target spatial domain and time period. No efforts therefore

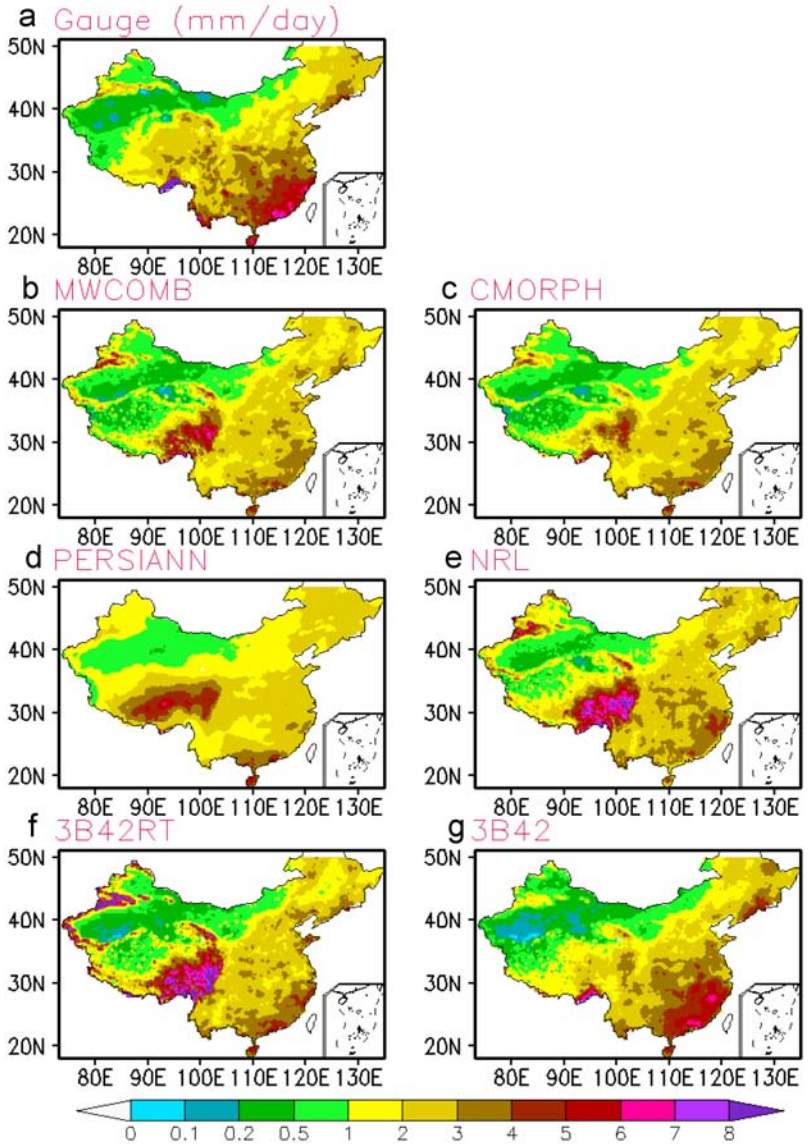

Figure 4. The 2005–2007 mean precipitation (mm d^{-1}) from (a) gauge-based analysis; (b) combined PMW estimates; (c) CMORPH; (d) PERSIANN; (e) NRL blended analysis; (f) TRMM 3B42 version 6, real time; and (g) TRMM 3B42 version 6.

are made in this work to quantify individual components of the error. This practice simplifies the examinations of satellite precipitation products and is adopted widely by many previous studies [e.g., *Ebert and Manton*, 1998; *Ebert et al.*, 2007; *Xie et al.*, 1996].

[28] In this study, gauge-based analyses, instead of reports of gauge measurements, are utilized to verify the satellite products. Defined by interpolating gauge measurements from nearby stations, spatial sampling error of the analyzed fields in representing precipitation over a grid box is usually smaller than that of the individual gauge reports. The quality of the gauge-based analysis relies heavily on the density and configuration of local station networks. In particular, gauge-based analyses of precipitation of a short accumulation period (e.g., 3 h) contain substantial inaccuracies over grid boxes where no station reports are available nearby. Results of the examinations are therefore compromised by the error in the gauge analysis. In this study, we try to perform the examinations of the satellite products using gauge analysis over grid boxes of 0.25° latitude/longitude when and where gauge reports from at least one station are available, ensuring that the comparison statistics reflect mostly the performance of satellite products.

4.1. Spatial Distribution and Seasonal Variations

[29] Figure 4 shows the spatial distribution of the 3 year mean precipitation from our hourly gauge analysis and the six satellite products. As shown in Figures 1 and 3, gauge reports of hourly precipitation over northern and western China are not available during cold seasons. Mean precipitation over those regions is therefore computed for warm seasons only. Precipitation distribution over China is characterized by a southeast-to-northwest decrease in the mean intensity. A large amount of precipitation is observed over southern and southeastern portions of the country where landfall of Typhoons and annual migration of the monsoon

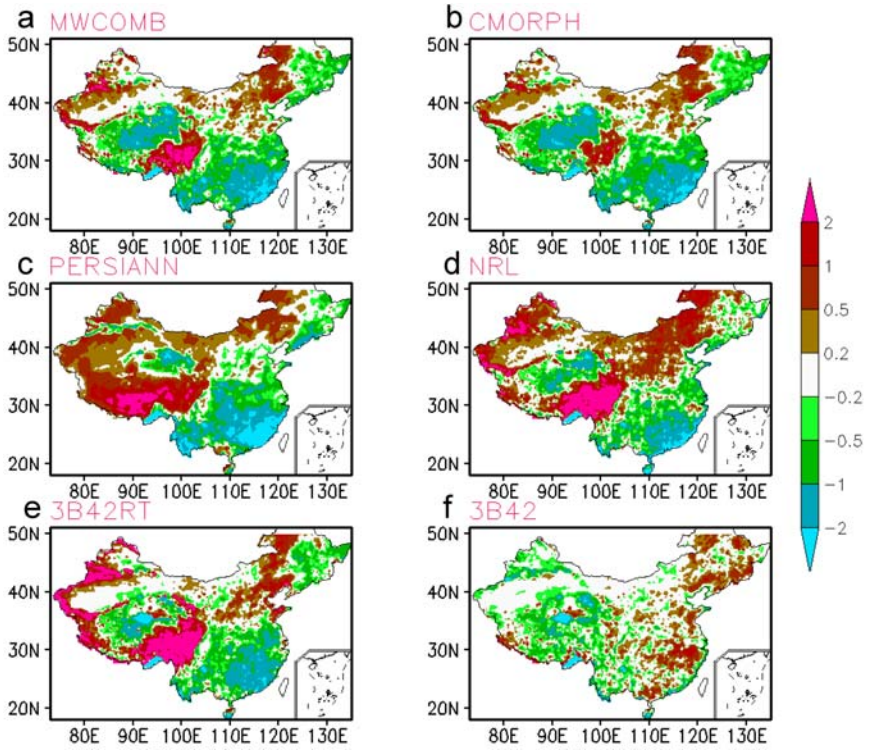

Figure 5. Bias (mm d^{-1}) in the 2005–2007 annual mean precipitation derived from high-resolution satellite precipitation products of (a) combined MW estimates; (b) CMORPH; (c) PERSIANN; (d) NRL blended analysis; (e) TRMM 3B42 version 6, real time; and (f) TRMM 3B42 version 6.

(Mei-Yu) bring in a lot of fresh water. Annual mean precipitation is very low, meanwhile, over the northwestern arid and semiarid regions.

[30] Temporal variations of precipitation estimated by the six satellite products are examined against those from the gauge-based analysis. While comparisons should be conducted over grid boxes with at least one gauge to ensure reasonable examinations of the satellite performance, displaying the resulting statistics over those sparsely distributed grid boxes would yield maps that are difficult to inspect and analyze. To facilitate an easy inspection of the spatial distributions of performance statistics, comparisons are conducted between the time series of satellite estimates and that of gauge analysis over all grid boxes (Figures 5, 6, and 7).

[31] All six satellite products depict the overall spatial patterns of 3 year mean precipitation very well. In particular, the gauge-adjusted satellite estimates of TRMM 3B42 exhibit close agreements with our gauge-based analysis. Satellite products with no gauge adjustments, however, present regional biases (Figure 5). They tend to underestimate the annual precipitation over southern and southeastern China, while giving overestimation over eastern Tibet and most of the regions in northwestern China. Given the fact that the microwave-only product (MWCOMB) shows bias of the same sign and close magnitude with that of the other PMW/IR blended products (CMORPH, PERSIANN, NRL, and TRMM 3B42RT), it is clear that bias over these regions are attributable mostly to that in the PMW estimates. The PERSIANN technique generates a huge mass of precipitation over the central and western Tibet plateau that is not visible in other satellite products and in the gauge analysis. A brief inspection of the PERSIANN reveals that the overestimation occurs mostly in winter and early spring and is associated with imperfect screening of the cold surface from the IR images (not shown). As described in section 2, hourly gauge reports are not collected over most of the north and western China. The "annual" mean precipitation shown in Figure 5 is therefore values averaged over all months during which both the gauge analysis and the satellite data are available.

[32] Figure 6 presents the spatial distribution of the serial correlation between our gauge-based analysis and the six satellite precipitation products on a 0.25° latitude/longitude and 3 hourly resolution. Reasonable correlation is observed over most of the region and for all of the satellite products examined here. Overall, satellite products exhibit better (worse) performance over regions with wet (dry) climatology. Serial correlation (correlation for time series) between the satellite and gauge data reaches 0.5 and higher for 3 hourly precipitation over southeastern China, while it is less than 0.2 over most regions in the northwest. Among the six satellite products, CMORPH shows the best correlation over most of the regions. Serial correlation for 3 hourly CMORPH is higher than 0.7 over some regions in the southeast China.

[33] The performance of satellite precipitation products improves as the averaging scale increases. The performance for estimates of precipitation averaged on 0.25° latitude/longitude and daily resolution (Figure 7) presents similar characteristics of spatial distribution but shows higher correlation over most of the regions. Serial correlation for

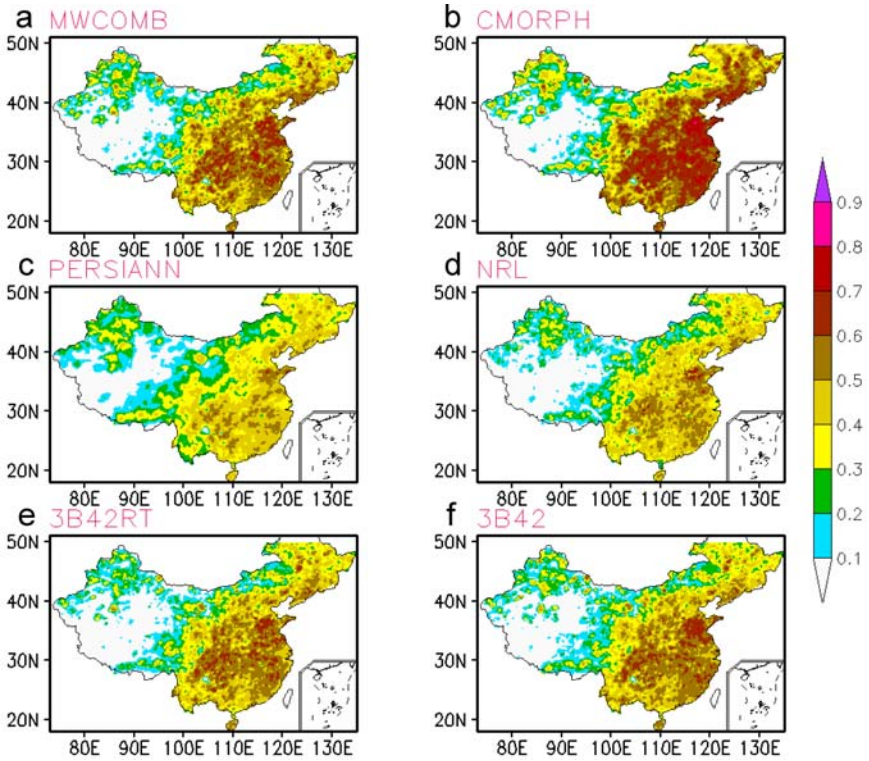

Figure 6. Serial correlation between gauge-based analysis of 3 hourly precipitation and that derived from the high-resolution precipitation products of (a) combined MW estimates; (b) CMORPH; (c) PERSIANN; (d) NRL blended analysis; (e) TRMM 3B42 version 6, real time; and (f) TRMM 3B42 version 6. Correlation is computed over a 3 year period from 2005 to 2007 using data when/where gauge analysis and all satellite estimates are available.

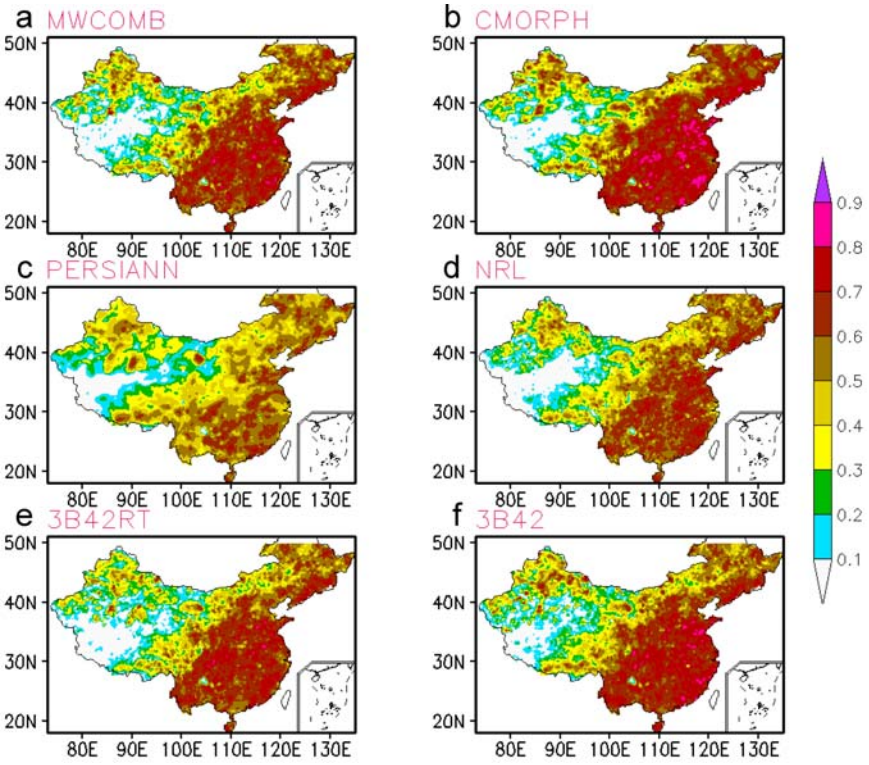

Figure 7. Same as in Figure 6, except for daily precipitation.

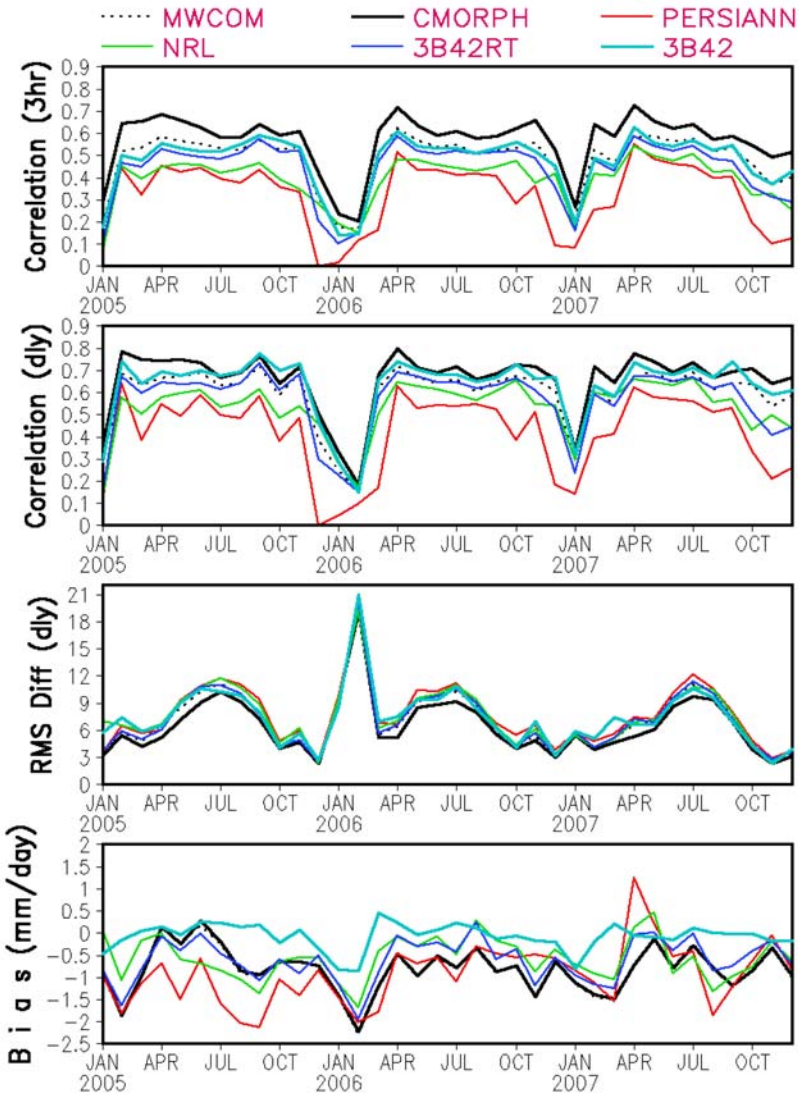

Figure 8. Time series of (a) pattern correlation between gauge-based analysis of 3 hourly precipitation and satellite products; (b) gauge-based analysis of daily precipitation and satellite products; (c) root mean square (RMS) differences (mm d^{-1}) between satellite products and gauge analysis; and (d) bias in the various satellite products. Statistics are computed using data over 0.25° latitude/longitude grid boxes where/when gauge reports are available from at least one station and satellite estimates generated by all satellite products.

daily CMORPH reaches 0.8 over many parts of southeastern China.

[34] To investigate how performance of the satellite precipitation changes with seasons, comparison statistics are calculated for each month during the 3 year period. Quality of the gauge-based analysis degrades over regions with a sparse station network [*Xie et al.*, 2007]. In particular, both bias and random error of substantial magnitude may occur in the gauge analysis over grid boxes with no station reports available nearby [*Chen et al.*, 2008]. To ensure reliable statistics, comparisons are conducted using gauge analysis and satellite data only over 0.25° latitude/longitude grid box where/when gauge reports are available from at least one station inside the grid box.

[35] Performance of satellite precipitation estimates exhibits distinct seasonal variations. Pattern correlation for the estimates of 3 hourly (Figure 8a) and daily precipitation (Figure 8b) is relatively low during cold seasons when the climate is dry and reaches a stable and higher level during mild and warm seasons starting from April to October. The root mean square differences (millimeters per day; see Figure 8c) between the satellite products and the gauge analysis are larger during warm seasons when rainfall is heavier. The CMORPH exhibits the best correlation with the gauge-based analysis throughout the 3 year comparison period, indicating its strong ability to reproduce the spatial distribution patterns of precipitation. The TRMM 3B42, a product defined by adjusting satellite-based estimates against the monthly gauge analysis of Global Precipitation Climatology Centre (GPCC) in Germany [*Schneider et al.*, 1993], presents the smallest biases compared to all other satellite products which under-estimate the mean precipita-

Table 1. Bias, Correlation, and Root Mean Square Differences Between Satellite Estimates and Gauge Observations of Precipitation on a 0.25° Latitude/Longitude Grid Over China for 2005–2007[a]

	Three Hours			Six Hours		Twelve Hours		Twenty-Four Hours	
	Bias (%)	Correlation	RMSD[b] (mm d^{-1})	Correlation	RMSD (mm d^{-1})	Correlation	RMSD (mm d^{-1})	Correlation	RMSD (mm d^{-1})
MWCOMB	−21.6	0.536	17.4	0.553	14.6	0.597	11.0	0.634	4.3
CMORPH	−20.8	0.604	15.1	0.632	12.4	0.656	9.8	0.684	4.0
PERSIANN	−26.0	0.415	17.1	0.455	14.1	0.481	11.4	0.514	4.8
NRL	−16.6	0.447	18.1	0.498	14.5	0.540	11.3	0.580	4.5
3B42RT	−15.0	0.502	19.8	0.558	15.0	0.589	11.2	0.624	4.3
3B42	−0.4	0.527	18.3	0.589	14.2	0.628	10.9	0.671	4.0

[a]The statistics are calculated over combined space and time domain using data over grid boxes where/when gauge observations are available from at least one station.

[b]RMSD, root mean square difference. RMSD is computed after the differences between the means of satellite estimates and gauge observations are removed. The mean gauge observed precipitation over the comparison period is 3.3 mm d^{-1}.

tion by ∼1 mm d^{-1} over China. The bias for CMORPH is also identical to that for the MWCOMB, a simple arithmetic mean of PMW estimates used as inputs to the CMORPH, indicating that the propagating and morphing processes in the CMORPH do not generate any mean error of significant amount.

[36] Table 1 summarizes the comparison statistics for the satellite products for precipitation estimates of different averaging periods. Since no gauge data are available during cold seasons over northern and western China, the comparison statistics reflect the overall performance of the satellite precipitation estimates of relatively mild climate. As expected, the agreement between satellite estimates and gauge observations improves with the averaging time scales. Correlation/root mean square differences (RMSD) between the MWCOMB and gauge observations are 0.536/17.4 mm d^{-1} for 3 hourly precipitation and reach 0.634/4.3 mm d^{-1} for daily accumulation. Here once again, CMORPH consistently shows the highest correlation and smallest RMS differences for all time scales examined here. The difference between the correlation/RMS for the CMORPH and those for other products, however, decreases with the increase of the averaging time scales of precipitation. Correlation for CMORPH/TRMM 3B42RT is 0.604/0.502 for 3 hourly precipitation, while it becomes 0.684/0.624 for daily precipitation, respectively. These results suggest that a Lagrangian approach like CMORPH works more effectively in defining precipitation maps of higher temporal resolution. Although only gauge analysis over grid boxes with reports from at least one station is included in the examination, the error statistics shown in Table 1 is still contaminated by the gauge analysis error especially over regions with relatively sparse gauge networks. Gauge analysis error needs to be quantified and removed from the statistics in future studies.

[37] TRMM 3B42 presents very small bias (−0.4%) compared to the gauge analysis. All other satellite products, meanwhile, exhibit biases of substantial magnitude, ranging from −15.0% for TRMM 3B42RT to −26.0% for PERSIANN. The contrasts in the bias for satellite products with and without gauge adjustment clearly demonstrated the importance and effectiveness of the gauge correction procedures. Even with a gauge analysis on a coarse spatial (1.0° latitude/longitude) and temporal (monthly) resolution derived from a relatively sparse station network (∼200 stations over China compared to ∼2000 used in our analysis), large-scale biases in the satellite estimates can be removed almost completely.

4.2. Probability Density Function of Precipitation Intensity

[38] In many applications, such as severe weather monitoring, land-atmospheric interactions, and hydrometeorological studies, accurate documentation for the frequencies of rainfall with different intensities is as important as that for the mean amount and spatial/temporal variation patterns of precipitation [*Tian et al.*, 2007]. The same amount of total precipitation may be attributable to weak rainfall of extended time period or heavy storms of short duration, yielding very different impacts in many aspects. In this section, we will examine how well the statistical characteristics of precipitation intensity are captured by the six high-resolution precipitation products.

[39] To this end, probability density function (PDF) of 3 hourly precipitation intensity over a 0.25° latitude/longitude grid box is computed for each of the six satellite products and compared against that derived from the gauge-based precipitation analysis for the 3 year period from 2005 to 2007. In considering the distribution characteristics of the 3 hourly precipitation, PDF is computed for 3 hourly precipitation intensity (R) of eight categories; that is, (1) no-rain (R = 0); (2) $0 < R \leq 0.5$ mm d^{-1}; (3) 0.5 mm $d^{-1} < R \leq 1.0$ mm d^{-1}; (4) 1.0 mm $d^{-1} < R \leq 2.0$ mm d^{-1}; (5) 2.0 mm $d^{-1} < R \leq 5.0$ mm d^{-1}; (6) 5.0 mm $d^{-1} < R \leq 10.0$ mm d^{-1}; (7) 10.0 mm $d^{-1} < R \leq 20.0$ mm d^{-1}; and (8) R > 20 mm d^{-1}.

[40] Over regions where gauge network is very sparse, the grid analysis of precipitation is computed from observations at distant stations, yielding an analysis of smooth distribution with enlarged raining areas [*Chen et al.*, 2008]. To ensure high quality of the PDF of gauge-based analysis to be used as the "truth," only data over grid boxes with at least one gauge report are included in the comparison.

[41] Figure 9 (top) shows the frequency of no-rain cases and the PDF of 3 hourly precipitation with various intensities, as observed by the gauge analysis and estimated by the six satellite products. In general, all satellite products examined here present reasonable PDF structures of 3 hourly precipitation intensity averaged over a grid box of 0.25° latitude/longitude grid box compared to those derived from the gauge-based analysis. The frequency of no-rain events, ∼84% as reported by the gauge analysis, is reproduced

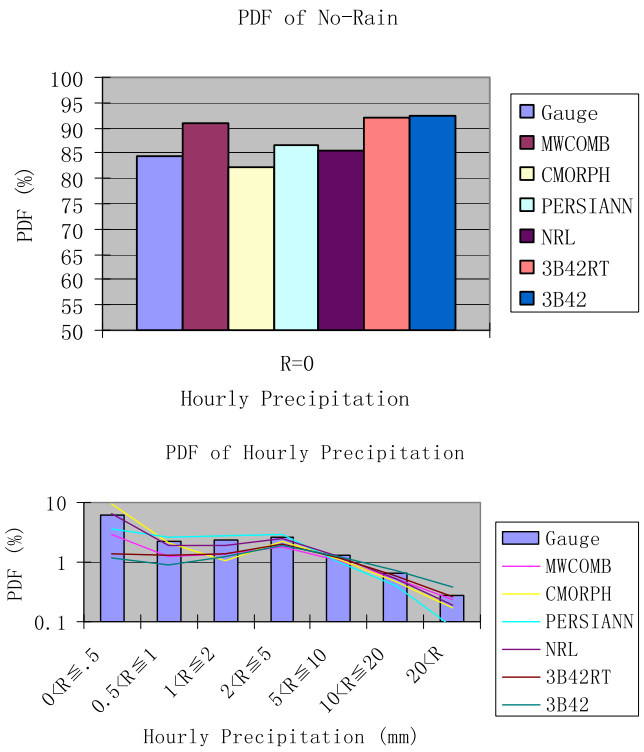

Figure 9. Probability density function (PDF) of 3 hourly precipitation for (top) no-rain cases and (bottom) for cases with precipitation of different intensities, as derived from the gauge analysis and various high-resolution satellite precipitation products.

well by all satellite products. All satellite products, except the CMORPH, however, tend to overestimate the frequency of no rain by several percent, indicating that satellite products miss some raining cases. The CMORPH and the NRL present the frequency of no-rain events closest to that of the observations.

[42] While all satellite products succeed in reproducing the overall PDF, they differ in their capacity in detecting precipitation of different intensities. CMORPH generates too many (few) points of light [<0.5 mm d^{-1}] (heavy rain [>20 mm d^{-1}]) cases, attributable, at least partially, to the morphing processes to define precipitation values as weighted mean of PMW estimates from multiple observations. The 3B42, meanwhile, over estimates the frequency of heavy precipitation cases. All other satellite products present under-estimate frequencies for both the light and heavy rain cases.

4.3. Diurnal Cycle

[43] The diurnal cycle of precipitation is one of the most important components of atmospheric variability, especially during warm seasons and over the tropics [*Dai and Deser*, 1999; *Lin et al.*, 2000; *Yang and Slingo*, 2001; *Sorooshian et al.*, 2002; *Pinker et al.*, 2006; *Dai et al.*, 2007]. Over China, previous studies using gauge observations have shown diurnal variations of substantial magnitude in the warm season precipitation associated with the monsoon (Mei-Yu) and heat convection [*Yu et al.*, 2007a, 2007b; *Zhou et al.*, 2008]. With their high spatial and temporal resolution, satellite precipitation products provide critical information useful to quantitatively document the diurnal variations of precipitation over the globe. In this section, we will examine the diurnal cycle of summer precipitation over China as depicted by our gauge-based analysis and the six high-resolution satellite products.

[44] Our gauge-based analysis of hourly precipitation shows large diurnal variations of summer (July–September (JAS)) precipitation, virtually over the entire contiguous China (Figure 10). Precipitation associated with the Mei-Yu system is organized as a band extending from central southern China over the east edge of the Tibet plateau northeasterly to central China and then turning easterly toward the east coast of China. Heavy precipitation is observed over the eastern edge of the Tibet plateau around local midnight (1500–1800 UT), propagating eastwardly along the front line and arriving at the east coast in the local afternoon (0900–1200 UT). Associated with this eastward phase propagation of the heavy precipitation, the diurnal cycle is observed with shifting phases along the Mei-Yu system. While this eastward phase propagation of the convection/precipitation has been detected by previous studies using cloud and rainfall data [*Wang et al.*, 2004; *Yu et al.*, 2007a], its underlying mechanisms remain the topic of investigation.

[45] Elsewhere over China, the diurnal variations of precipitation appear more localized. Particularly noticeable is the diurnal cycle associated with the heat convection over the coastal regions of southern and southeastern China (Figure 10). Convective precipitation starts from early morning around 0500–0800 local standard time (LST) (2100–2400 geomagnetic time (GMT)), reaches its maximum in late afternoon around 1700–1900 LST (0900–1200 GMT), and then decays quickly afterward.

[46] Generally speaking, the high-resolution satellite precipitation products are capable of detecting the overall features of the diurnal variations observed by the gauge analysis (Figure 11). The eastward phase propagation of the heavy precipitation along the Mei-Yu frontal system is captured quite well, though precipitation intensity in the local afternoon (0900–1200 GMT) over the east edge of the Tibet plateau is overestimated. The diurnal variations over the coastal regions, northern China and northwestern China are also well represented by the satellite products.

[47] More quantitative examinations of the diurnal variations of precipitation are performed for two selected regions: a coastal region over Zhejiang Province in southern China (119 to 122°E; 26 to −30°N) and a central eastern China region covered by the Mei-Yu system (116–122°E; 31–35°N). Presented in Figure 12 are mean diurnal cycle of 2005–2007 JAS precipitation averaged over the regions dominated by heat convection (Figures 12a and 12c) and Mei-Yu system (Figures 12b and 12d). Mean precipitation values of satellite estimates and gauge analysis computed for 3 hourly boxes starting/ending and centered at 0000–2100 UT are plotted in Figures 12a and 12c. Precipitation variations during the July–September (JAS) season are dominated by the diurnal cycle over the southeastern coastal region (Figures 12a and 12c). The amplitude of the precipitation diurnal cycle, as observed by the gauge analysis, is ~5.8 mm d^{-1}, more than 90% of the daily mean (6.3 mm d^{-1}). The minimum/maximum amount of precipitation

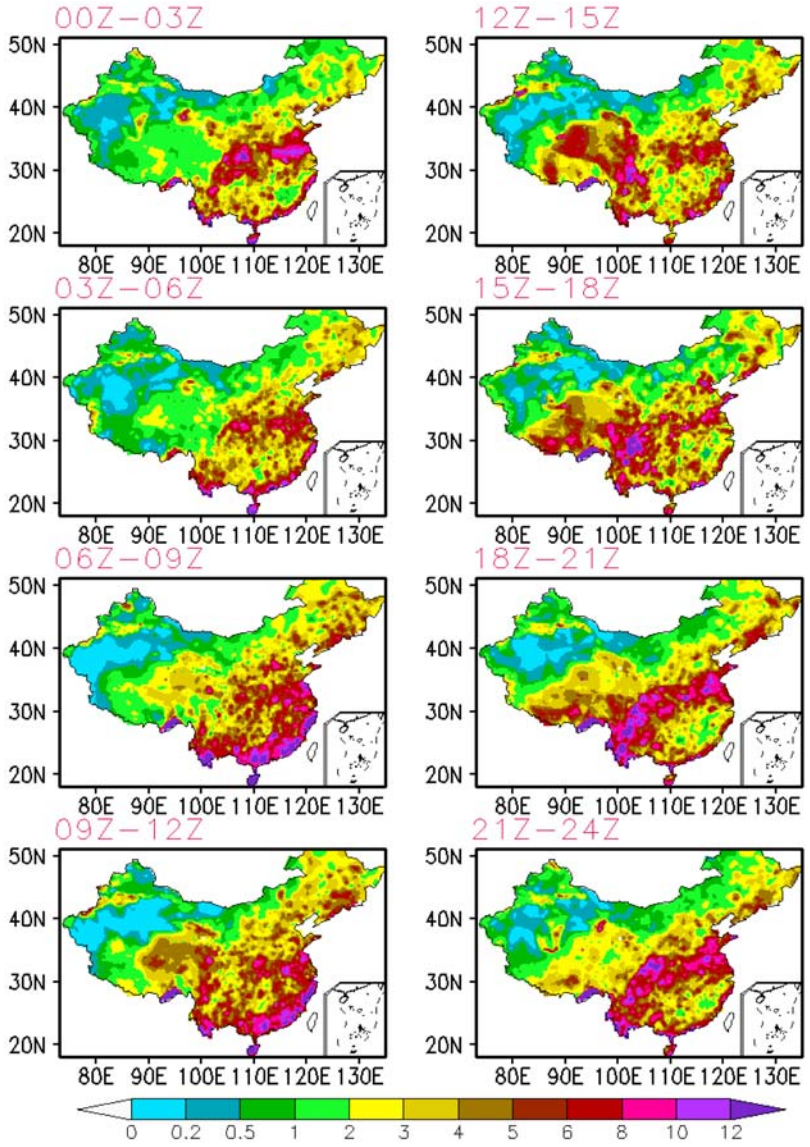

Figure 10. Warm season mean diurnal cycle of precipitation (mm d^{-1}) derived from our gauge-based analysis for July–September over 2005–2007.

appears in the local morning (~5000 LST) and afternoon (~1700 LST). All satellite products present mean diurnal changes of precipitation in close agreement with those of the gauge analysis in both the phase and relative amplitude. All of the satellite products, with the exception of the gauge-adjusted TRMM 3B42, tend to under-estimate the total precipitation amount, consistent with our findings described in section 4.1. The TRMM 3B42 gives quite accurate estimation of the daily mean precipitation but overestimates/under-estimates the maximum/minimum values, yielding a diurnal cycle with slightly larger amplitude. The diurnal peak in the NRL blended product is ~1–3 h earlier than that in the gauge analysis. The validation results for the diurnal cycle are in broad agreement with those of *Liang and Xie* [2007], who compared the high-resolution satellite precipitation estimates with a gauge analysis over Guang-Dong Province in southern China.

[48] For the eastern part of the Mei-Yu system over central eastern China, summer precipitation shows a diurnal cycle of relatively small amplitude (~30% of the daily mean) and a double-peak pattern, one in the early morning and the other in the afternoon (Figures 12b and 12d). *Yu et al.* [2007b] examined the Mei-Yu related precipitation diurnal variations in the same regions and found that the early morning and afternoon peaks are attributable mostly to rainfall events of long (>6 h) and short duration (<6 h), respectively.

[49] All satellite precipitation products captured the afternoon peak very well. The precipitation peak in the early morning as observed by the gauge analysis, however, is substantially under-estimated in the satellite estimates. This is consistent with the finding of *Zhou et al.* [2008] who evaluated the PERSIANN and TRMM 3B42 data sets for a 5 year period from 2000 to 2004. The causes of this under-estimation need to be identified by future research. Since the morning peak is associated with precipitation of extended duration [*Yu et al.*, 2007b], precipitation from large-scale stratocumulus clouds, which is more difficult to detect from

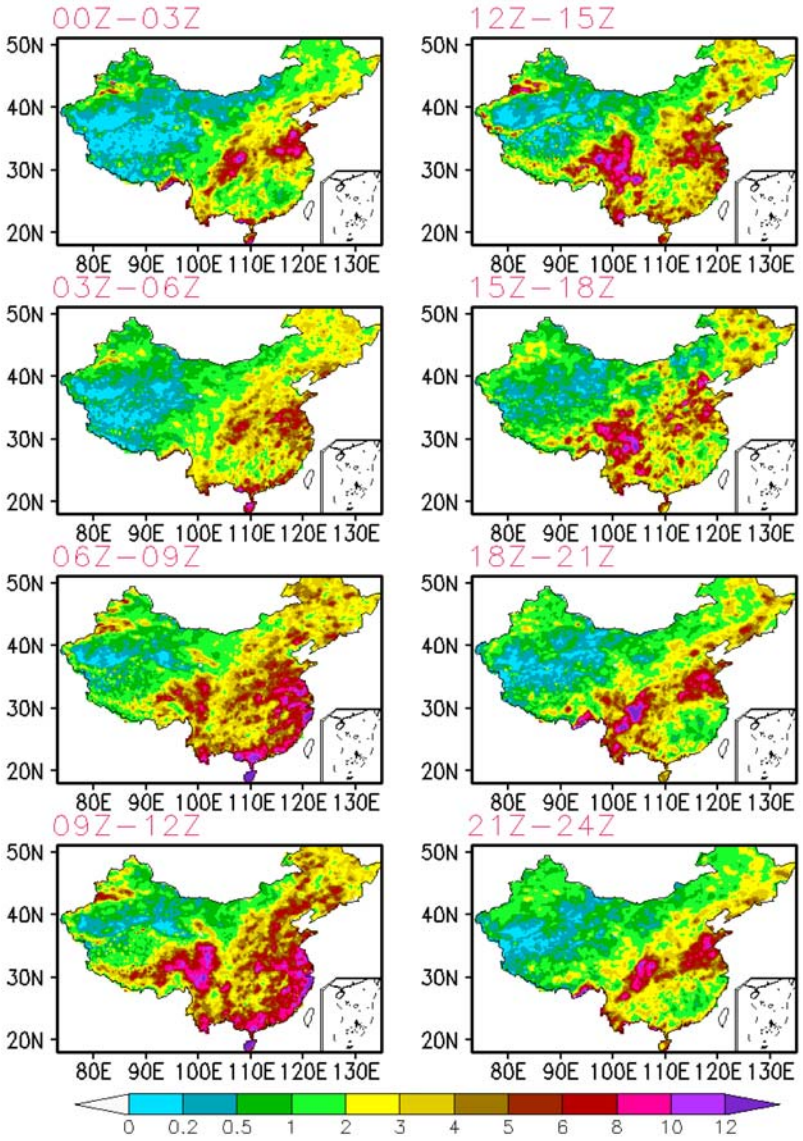

Figure 11. Same as in Figure 10, except for mean diurnal cycle derived from CMORPH satellite estimates.

most operational passive microwave (PMW) instruments, may be involved.

5. Summary and Conclusions

[50] A gauge-based analysis of hourly precipitation is constructed on a 0.25° latitude/longitude grid over the contiguous China for a 3 year period from 2005 to 2007 by interpolation of gauge reports from ~2000 stations. The station data used here are collected and quality controlled by the National Meteorological Information Center (NMIC) of the China Meteorological Administration (CMA). The objective analysis technique applied here is a modification of *Xie et al.* [2007] which defines analyzed value of precipitation through the optimal interpolation (OI) method with consideration of orographic effects.

[51] The hourly gauge analysis is applied to examine the performance of six high-resolution satellite precipitation products, including the PERSIANN, NRL, CMORPH, MWCOMB, TRMM 3B42, and TRMM 3B42RT, with an emphasis on the evaluation of the satellite products' capability to capture precipitation variations of subdaily time scales. Our comparison results showed the following:

[52] 1. All of the six high-resolution satellite products are capable of capturing the overall spatial distribution and temporal variation patterns of precipitation with reasonable quality.

[53] 2. Performance of the satellite products varies for different regions and different precipitation regimes, with better agreements for precipitation in the warm seasons and over wet regions.

[54] 3. All products based solely on satellite observations present regionally and seasonally varying biases, while the gauge-adjustment procedures included in the TRMM 3B42 remove the large-scale bias almost completely.

[55] 4. Among all the satellite products examined, the CMORPH exhibits the best performance in depicting the spatial pattern and temporal variations of precipitation.

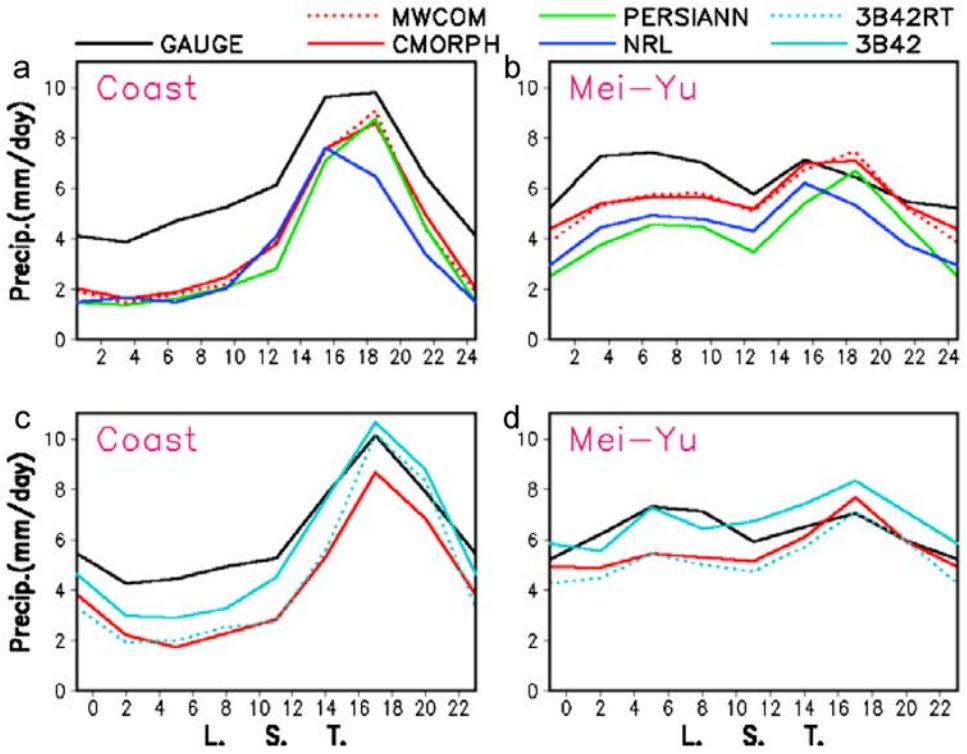

Figure 12. Warm season (July–September) mean diurnal cycle of precipitation (mm d^{-1}) over two regions dominated by the coastal convection (Figures 12a and 12c) and Mei-Yu system (Figures 12b and 12d). Results derived from 3 hourly precipitation estimates, starting and centering at 0000, 0300, ... 2100 UT are plotted.

[56] 5. Both the relative magnitude and the phase of the warm season precipitation over China are estimated quite well by the satellite products, but the early morning peak associated with the Mei-Yu rainfall over central eastern China is substantially under-estimated.

[57] Techniques to construct high-resolution precipitation estimates through integration of information from multiple satellites are evolving rapidly in recent years. Assessment results presented in this study represent, at most, the status of the satellite products for the 3 year period from 2005 to 2007. Substantial progress has been made since then to improve the input data reprocessing procedures and refine the combining algorithms. An important aspect of the satellite products development is the continued examination of the precipitation estimates over various regions of the globe. We will continue our efforts in this respect to provide up-to-date information about the performance of high-resolution satellite precipitation products over China.

[58] The work reported in this paper is an integral part of a CMA/NMIC effort to construct a suite of gauge-based and gauge-satellite merged precipitation products for operational and research applications. Further work is underway to take advantage of the error structure of the satellite products we defined in this study to create an analysis of precipitation by merging information from gauge observations and satellite estimates.

[59] **Acknowledgments.** This work is supported by the Construction of an Analysis, Data Storage and Sharing System for the East Asia Climate Program (GYHY(QX)2-7-6-5) of the China Meteorological Administration. The authors would like to thank Lin Zhou, Zijiang Zhou, and Yingrui Sun at the National Meteorological Information Center of the China Meteorological Administration for their encouragement and support of this work. Discussions with Jian-Yin Liang led to a refined research strategy for the work described in this paper. Comments from three anonymous reviewers helped improve greatly the quality of this paper.

References

Adler, R. F., C. Kidd, G. Petty, M. Morrissey, and H. M. Goodman (2001), Intercomparison of global precipitation products: The third Precipitation Intercomparison Project (PIP-3), *Bull. Am. Meteorol. Soc.*, *82*, 1377–1396, doi:10.1175/1520-0477(2001)082<1377:IOGPPT>2.3.CO;2.

Arkin, P. A., and B. N. Meisner (1987), The relationship between large-scale convective rainfall and cold cloud cover over the western hemisphere during 1982–1984, *Mon. Weather Rev.*, *115*, 51–74, doi:10.1175/1520-0493(1987)115<0051:TRBLSC>2.0.CO;2.

Bell, T. L., and P. K. Kundu (2003), Comparing satellite rainfall estimates with rain gauge data: Optimal strategies suggested by a spectral model, *J. Geophys. Res.*, *108*(D3), 4121, doi:10.1029/2002JD002641.

Bowman, K. P. (2005), Comparison of TRMM precipitation retrievals with rain gauge data from ocean buoys, *J. Clim.*, *18*, 178–190, doi:10.1175/JCLI3259.1.

Bowman, K. P., A. B. Phillips, and G. R. North (2003), Comparison of TRMM rainfall retrievals with rain gauge data from the TAO/TRITON buoy array, *Geophys. Res. Lett.*, *30*(14), 1757, doi:10.1029/2003GL017552.

Chen, M., P. Xie, J. E. Janowiak, and P. A. Arkin (2002), Global land precipitation: A 50-year monthly analysis based on gauge observations, *J. Hydrometeorol.*, *3*, 249–266, doi:10.1175/1525-7541(2002)003<0249:GLPAYM>2.0.CO;2.

Chen, M., W. Shi, P. Xie, V. B. S. Silva, V. E. Kousky, R. Wayne Higgins, and J. E. Janowiak (2008), Assessing objective techniques for gauge-based analyses of global daily precipitation, *J. Geophys. Res.*, *113*, D04110, doi:10.1029/2007JD009132.

Dai, A. (2006), Precipitation characteristics in eighteen coupled climate models, *J. Clim.*, *19*, 4605–4630, doi:10.1175/JCLI3884.1.

Dai, A., and C. Deser (1999), Diurnal and semidiurnal variations in global surface wind and divergence fields, *J. Geophys. Res.*, *104*, 31,109–31,125, doi:10.1029/1999JD900927.

Dai, A., I. Y. Fung, and A. D. del Genio (1997), Surface observed global land precipitation variations during 1900–88, *J. Clim.*, *10*, 2943–2962, doi:10.1175/1520-0442(1997)010<2943:SOGLPV>2.0.CO;2.

Dai, A., F. Giorgi, and K. E. Trenberth (1999), Observed and model simulated diurnal cycles of precipitation over the United States, *J. Geophys. Res.*, *104*, 6377–6402, doi:10.1029/98JD02720.

Dai, A., X. Lin, and K. Hsu (2007), The frequency, intensity, and diurnal cycle of precipitation in surface and satellite observations over low- and mid-latitudes, *Clim. Dyn.*, *29*, 727–744, doi:10.1007/s00382-007-0260-y.

Daly, C., R. P. Neilsen, and D. L. Phillips (1994), A statistical-topographic model for mapping climatological precipitation over mountainous terrain, *J. Appl. Meteorol.*, *33*, 140–158, doi:10.1175/1520-0450(1994)033<0140:ASTMFM>2.0.CO;2.

Ebert, E. E., and M. J. Manton (1998), Performance of satellite rainfall estimation algorithms during TOGA COARE, *J. Atmos. Sci.*, *55*, 1537–1557, doi:10.1175/1520-0469(1998)055<1537:POSREA>2.0.CO;2.

Ebert, E. E., J. E. Janowiak, and C. Kidd (2007), Comparison of near-real-time precipitation estimates from satellite observations and numerical models, *Bull. Am. Meteorol. Soc.*, *88*, 47–64, doi:10.1175/BAMS-88-1-47.

Ferraro, R. R. (1997), Special sensor microwave imager derived global rainfall estimates for climatological applications, *J. Geophys. Res.*, *102*, 16,715–16,735.

Gandin, L. S. (1965), *Objective Analysis of Meteorological Fields*, 242 pp., Isr. Program for Sci. Transl., Jerusalem.

Gottschalck, J., J. Meng, M. Rodell, and P. Houser (2005), Analysis of multiple precipitation products and preliminary assessment of their impact on Global Land Data Assimilation System land surface states, *J. Hydrometeorol.*, *6*, 573–598, doi:10.1175/JHM437.1.

Hammer, G. R., and P. M. Steurer (1997), Data set documentation for hourly precipitation data, *Rep. TD3240*, 18 pp., NOAA Natl. Clim. Data Cent., Asheville, N. C. (Available as ftp://ftp.ncdc.noaa.gov/pub/data/documentlibrary/tddoc/td3240.doc)

Higgins, R. W., J. E. Janowiak, and Y.-P. Yao (1996), *A Gridded Hourly Precipitation Data Base for the United States (1963–1993), NCEP Clim. Predict. Cent. Atlas 1*, U.S. Dep. of Commer., NOAA, Camp Springs, Md.

Higgins, R. W., W. Shi, E. Yarosh, and R. Joyce (2000), *Improved United States Precipitation Quality Control System and Analysis, NCEP Clim. Predict. Cent. Atlas 7*, U.S. Dep. of Commer., NOAA, Camp Springs, Md.

Hong, Y., D. Glchis, J.-T. Cheng, K.-L. Hsu, and S. Sorooshian (2007), Evaluation of PERSIANN-CCS rainfall measurement using the NAME event rain gauge network, *J. Hydrometeorol.*, *8*, 469–482, doi:10.1175/JHM574.1.

Hossain, F., and E. N. Anagnostou (2004), Assessment of current passive-microwave- and infrared-based satellite rainfall remote sensing for flood prediction, *J. Geophys. Res.*, *109*, D07102, doi:10.1029/2003JD003986.

Hsu, K.-L., X. Gao, S. Sorooshian, and V. Gupta (1997), Precipitation estimation from remotely sensed information using artificial neural networks, *J. Appl. Meteorol.*, *36*, 1176–1190, doi:10.1175/1520-0450(1997)036<1176:PEFRSI>2.0.CO;2.

Huffman, G. J., R. F. Adler, D. T. Bolvin, G. Gu, E. J. Nelkin, Y. Hong, and D. B. Wolff (2007), The TRMM multisatellite precipitation analysis (TMPA): Quasi-global, multiyear, combined-sensor precipitation estimates at fine scales, *J. Hydrometeorol.*, *8*, 38–55, doi:10.1175/JHM560.1.

Hulme, M. (1991), An intercomparison of model and observed global precipitation climatologies, *Geophys. Res. Lett.*, *18*, 1715–1718, doi:10.1029/91GL01850.

Janowiak, J. E., V. E. Kousky, and R. J. Joyce (2005), Diurnal cycle of precipitation determined from the CMORPH high spatial and temporal resolution global precipitation analyses, *J. Geophys. Res.*, *110*, D23105, doi:10.1029/2005JD006156.

Joyce, R. J., J. E. Janowiak, P. A. Arkin, and P. Xie (2004), CMORPH: A method that produces global precipitation estimates from passive microwave and infrared data at high spatial and temporal resolution, *J. Hydrometeorol.*, *5*, 487–503, doi:10.1175/1525-7541(2004)005<0487:CAMTPG>2.0.CO;2.

Kummerow, C., et al. (2000), The status of the Tropical Rainfall Measuring Mission (TRMM) after two years in orbit, *J. Appl. Meteorol.*, *39*, 1965–1982, doi:10.1175/1520-0450(2001)040<1965:TSOTTR>2.0.CO;2.

Legates, D. R., and C. J. Willmott (1990), Mean seasonal and spatial variability in gauge-corrected, global precipitation, *Int. J. Climatol.*, *10*, 111–127, doi:10.1002/joc.3370100202.

Liang, J.-Y., and P. Xie (2007), Verifying high-resolution satellite precipitation estimates on sub-daily time scales: Results for southern China, paper presented at 21st Conference on Hydrology, Am. Meteorol. Soc., Atlanta, Ga., 15–18 January.

Liang, X.-Z., L. Li, A. Dai, and K. E. Kunkel (2004), Regional climate model simulation of summer precipitation diurnal cycle over the United States, *Geophys. Res. Lett.*, *31*, L24208, doi:10.1029/2004GL021054.

Lin, X., D. A. Randall, and L. D. Fowler (2000), Diurnal variability of the hydrologic cycle and radiative fluxes: Comparisons between observations and a GCM, *J. Clim.*, *13*, 4159–4179, doi:10.1175/1520-0442(2000)013<4159:DVOTHC>2.0.CO;2.

McCollum, J., W. F. Krajewski, R. R. Ferraro, and M. B. Ba (2002), Evaluation of biases of satellite rainfall estimation algorithms over the continental United States, *J. Appl. Meteorol.*, *41*, 1065–1080, doi:10.1175/1520-0450(2002)041<1065:EOBOSR>2.0.CO;2.

Morrissey, M. L., J. A. Maliekal, J. S. Greene, and J. Wang (1995), The uncertainty of simple spatial averages using rain gauge networks, *Water Resour. Res.*, *31*, 2011–2017, doi:10.1029/95WR01232.

Nesbitt, S. W., and E. J. Zipser (2003), The diurnal cycle of rainfall and convective intensity according to three years of TRMM measurements, *J. Clim.*, *16*, 1456–1475.

New, M. G., M. Hulme, and P. D. Jones (1999), Representing twentieth-century space-time climate variability. part I: Development of a 1961–90 mean monthly terrestrial climatology, *J. Clim.*, *12*, 829–856, doi:10.1175/1520-0442(1999)012<0829:RTCSTC>2.0.CO;2.

New, M. G., M. Hulme, and P. D. Jones (2000), Representing twentieth-century space-time climate variability. part II: Development of 1901–96 monthly grids of terrestrial climatology, *J. Clim.*, *13*, 2217–2238, doi:10.1175/1520-0442(2000)013<2217:RTCSTC>2.0.CO;2.

Pinker, R. T., Y. Zhao, C. Akoshile, J. Janowiak, and P. A. Arkin (2006), Diurnal and seasonal variability of rainfall in the sub-Sahel as seen from observations, satellites, and a numerical model, *Geophys. Res. Lett.*, *33*, L07806, doi:10.1029/2005GL025192.

Schneider, U., B. Rudolf, and W. Ruth (1993), The spatial sampling error of areal mean monthly mean precipitation totals analyzed from gauge measurements, in *4th International Conference on Precipitation*, edited by G. Slinn, pp. 80–82, Elsevier, New York.

Serra, Y. L., and M. J. McPhaden (2003), Multiple time and space comparisons of atlas buoy rain gauge measurements with TRMM satellite precipitation measurements, *J. Appl. Meteorol.*, *42*, 1045–1059, doi:10.1175/1520-0450(2003)042<1045:MTASCO>2.0.CO;2.

Sorooshian, S., X. Gao, R. A. Maddox, Y. Hong, and B. Iman (2002), Diurnal variability of tropical precipitation retrieved from combined GOES and TRMM satellite information, *J. Clim.*, *15*, 983–1001, doi:10.1175/1520-0442(2002)015<0983:DVOTRR>2.0.CO;2.

Spencer, R. W. (1993), Global oceanic precipitation from MSU during 1979–91 and comparisons to other climatologies, *J. Clim.*, *6*, 1301–1326, doi:10.1175/1520-0442(1993)006<1301:GOPFTM>2.0.CO;2.

Susskind, J., P. Piraino, L. Rokkle, and A. Mehta (1997), Characteristics of the TOVS Pathfinder Path A dataset, *Bull. Am. Meteorol. Soc.*, *78*, 1449–1472, doi:10.1175/1520-0477(1997)078<1449:COTTPP>2.0.CO;2.

Tian, Y., C. D. Peters-Lidard, B. J. Choudhury, and M. Garcia (2007), Multitemporal analysis of TRMM-based satellite precipitation products for land data assimilation applications, *J. Hydrometeorol.*, *8*, 1165–1183, doi:10.1175/2007JHM859.1.

Turk, F. J., E. E. Ebert, B.-J. Sohn, H.-J. Oh, V. Levizzani, E. A. Smith, and R. Ferraro (2004), Validation of an operational global precipitation analysis at short time scales, paper presented at 12th Conference on Satellite Meteorology and Oceanography, Am. Meteorol. Soc., Seattle, Wash., 11–15 Jan.

Ushio, T., et al. (2009), A Kalman filter approach to the Global Satellite Mapping of Precipitation (GSMaP) from combined passive microwave and infrared radiometric data, *J. Meteorol. Soc. Jpn.*, *87A*, 137–151.

Wang, C. C., G. T. J. Chen, and R. E. Carbone (2004), A climatology of warm-season cloud patterns over East Asia based on GMS infrared brightness temperature observations, *Mon. Weather Rev.*, *132*, 1606–1629, doi:10.1175/1520-0493(2004)132<1606:ACOWCP>2.0.CO;2.

Wilheit, T. J., A. T. C. Chang, and L. S. Chiu (1991), Retrieval of the monthly rainfall indices from microwave radiometric measurements using probability distribution functions, *J. Atmos. Oceanic Technol.*, *4*, 264–282.

Xie, P., and P. A. Arkin (1998), Global monthly precipitation estimates from satellite-observed outgoing longwave radiation, *J. Clim.*, *11*, 137–164, doi:10.1175/1520-0442(1998)011<0137:GMPEFS>2.0.CO;2.

Xie, P., B. Rudolf, U. Schneider, and P. A. Arkin (1996), Gauge-based monthly analysis of global land precipitation from 1971 to 1994, *J. Geophys. Res.*, *101*, 19,023–19,034, doi:10.1029/96JD01553.

Xie, P., M. Chen, A. Yatagai, T. Hayasaka, Y. Fukushima, and S. Yang (2007), A gauge-based analysis of daily precipitation over East Asia, *J. Hydrometeorol.*, *8*, 607–626, doi:10.1175/JHM583.1.

Yang, G., and J. Slingo (2001), The diurnal cycle in the tropics, *Mon. Weather Rev.*, *129*, 784–801, doi:10.1175/1520-0493(2001)129<0784:TDCITT>2.0.CO;2.

Yang, S., and E. A. Smith (2006), Mechanisms for diurnal variability of global tropical precipitation observed from TRMM, *J. Clim.*, *19*, 5190–5226, doi:10.1175/JCLI3883.1.

Yu, R., B. Wang, and T. Zhou (2004), Climate effects of the deep continental stratus clouds generated by the Tibetan plateau, *J. Clim.*, *17*, 2702–2713, doi:10.1175/1520-0442(2004)017<2702:CEOTDC>2.0.CO;2.

Yu, R., T. Zhou, A. Xiong, Y. Zhu, and J. Li (2007a), Diurnal variations of summer precipitation over contiguous China, *Geophys. Res. Lett.*, *34*, L01704, doi:10.1029/2006GL028129.

Yu, R., Y. Xu, T. Zhou, and J. Li (2007b), Relation between rainfall duration and diurnal cycle in the warm season precipitation over central eastern China, *Geophys. Res. Lett.*, *34*, L13703, doi:10.1029/2007GL030315.

Zhou, T., R. Yu, H. Chen, A. Dai, and Y. Pan (2008), Summer precipitation frequency, intensity, and diurnal cycle over China: A comparison of satellite data with rain gauge observations, *J. Clim.*, *21*, 3997–4010, doi:10.1175/2008JCLI2028.1.

Y. Shen, Y. Wang, and A. Xiong, National Meteorological Information Center, China Meteorological Administration, 46 Zhongguancun South Ave., Haidian District, Beijing 100081, China. (sheny@cma.gov.cn)

P. Xie, NOAA Climate Prediction Center, 5200 Auth Rd., Room 605, Camp Springs, MD 20746, USA.